

# Quantum Sensing using Geometrical Phase in Qubit-Oscillator Systems

Nishchay Suri,<sup>1,\*</sup> Zhihui Wang,<sup>2,3</sup> Tanay Roy,<sup>4</sup> Davide Venturelli,<sup>2,3</sup> and Wibe Albert de Jong<sup>1</sup>

<sup>1</sup>*Applied Mathematics and Computational Research Division,*

*Lawrence Berkeley National Laboratory, Berkeley, California 94720, USA*

<sup>2</sup>*Quantum Artificial Intelligence Laboratory, NASA Ames Research Center, Moffett Field, CA 94035, USA*

<sup>3</sup>*USRA Research Institute for Advanced Computer Science, Mountain View, California 94043, USA*

<sup>4</sup>*Superconducting Quantum Materials and Systems (SQMS) Center,  
Fermi National Accelerator Laboratory (FNAL), Batavia, IL 60510, USA*

We present a quantum sensing protocol for coupled qubit-oscillator systems that surpasses the standard quantum limit (SQL) by exploiting a geometrical phase. The signal is encoded in the geometrical phase that is proportional to the area enclosed in oscillator phase space. This area is amplified through squeezing, enabling sensitivities beyond the SQL. Our method is independent of oscillator's initial state, amenable to sensing with high-temperature or logical error-corrected states. The protocol shows robustness to qubit Markovian noise and preserves its state-independence, underscoring its practicality for next-generation quantum metrology. We demonstrate application to force sensing beyond the SQL in longitudinally coupled systems, and to high-precision measurements of couplings and pulse calibration surpassing SQL in dispersively coupled circuit quantum electrodynamics (cQED) architectures.

*Introduction*— Quantum technologies have seen remarkable progress in recent years, especially in the field of quantum computing and information processing. Qubit-oscillator systems are ubiquitous in this landscape, forming the basis of architectures ranging from superconducting circuits and trapped ions to optomechanical, spin-mechanical, and semiconductor devices [1–5]. These systems combine the exceptional force sensitivity of the oscillator with the precise control and high-fidelity readout of the qubit, making them a versatile platform for sensing [6–11]. The architecture has been proposed for a wide range of applications that include inertial-force sensing (such as gravimetry) and tests for macroscopic superposition in levitated NV centers [12–15] and superconducting spheres [16–20], magnetometry [21–24], electromechanical sensing in circuit-quantum electrodynamics (cQED) [25–30] and dark matter detection [31–35].

Squeezing the oscillator quadrature is a cornerstone of quantum sensing, enabling measurement sensitivities beyond classical or the standard quantum limit (SQL) [36, 37]. This capability has opened the door to key experiments probing fundamental physics [38–40]. It is therefore desirable to seek a protocol that combines the high-fidelity qubit readout with the sensitivity enhancement provided by squeezing. However, we show that although a straightforward application of squeezing amplifies the signal, the resulting enhancement is undetectable through standard qubit measurements.

In this Letter, we introduce a quantum sensing protocol for coupled qubit-oscillator systems that encodes the signal in a detectable geometrical phase. Importantly, this geometrical phase is proportional to the area enclosed by the oscillator motion in its phase space. Using the insight that squeezing is a geometrical operation that can amplify the oscillator path [41] and therefore the area, our protocol enables sensitivities beyond the

SQL. While geometric phases in bosonic systems have been extensively studied [42–44], applied to pulse calibration [45], engineering entangling gates [46, 47], and even for generating entangled states for sensing [48], here, we exploit the geometric nature of the phase, specifically, its proportionality to enclosed area to amplify sensitivity. We first apply our method to longitudinally coupled systems for inertial force sensing such as gravimetry and then extend it to precision measurement of couplings and pulse calibration in cQED systems that are dispersively coupled. Since the phase is accumulated along a closed loop in oscillator phase space, our protocol is independent of the oscillator's initial state, allowing operation with high-temperature thermal states and compatibility with bosonic error-correcting codes such as GKP states [49–51]—opening pathways to fault-tolerant quantum sensing. Finally, we analyze the dynamics under Markovian noise affecting both qubit and oscillator, showing that the protocol retains its state-independence and robustness under qubit noise, underscoring its practicality for a broad range of next-generation quantum metrology applications.

*Sensing in longitudinally-coupled systems*— We first discuss detection of force by measuring the qubit in longitudinally coupled qubit-oscillator (see Fig. 1(a)) systems [12–30, 52–54]. The Hamiltonian in the lab frame is given by

$$\frac{H_L}{\hbar} = -\frac{\omega_q}{2} \hat{\sigma}_z + \omega \hat{a}^\dagger \hat{a} + \gamma (\hat{a} + \hat{a}^\dagger) \sigma_z + \eta (\hat{a} + \hat{a}^\dagger), \quad (1)$$

where  $\omega_q$  is the qubit frequency,  $\omega$  is the oscillator frequency,  $\gamma$  is the longitudinal coupling strength, and  $\eta = F/\sqrt{2m\omega\hbar}$  encodes an unknown weak force  $F$  acting on the oscillator with mass  $m$ . Since  $\hat{\sigma}_z$  commutes with  $H_L$ , we work in its eigen-basis with eigenvalues  $s = \pm 1$  corresponding to eigenstates  $\{|\uparrow\rangle, |\downarrow\rangle\}$ . For each qubit state  $|s\rangle$ , the time evolution in the frame rotating with

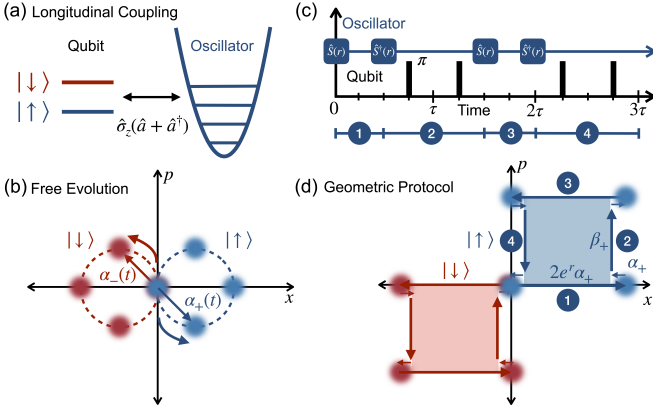


FIG. 1. We consider (a) longitudinally-coupled qubit-oscillator systems. (b) Free evolution of the coupled system in the oscillator phase space. (c) Sequence of operations on the oscillator and qubit for the geometric protocol and (d) the corresponding phase space motion.

qubit and oscillator is given by [55]

$$\hat{U}_s(t) = e^{is\frac{\phi(t)}{2}} \hat{D}(\alpha_s(t)), \quad (2)$$

during which the qubit state acquires a relative phase  $\phi(t) = 4\eta\gamma(\omega t - \sin\omega t)/\omega$ , and the oscillator traces a circular path with displacement  $\alpha_s(t) = \alpha_s(1 - e^{i\omega t})$  where  $\alpha_s = (\eta + \gamma s)/\omega$ , as shown in Fig. 1(b). Proposed sensing protocols [12–19] estimate the force by measuring the phase  $\phi(t)$  using an interference experiment. We briefly summarize this free-evolution scheme in the following. The system is prepared in a product state  $|\psi(0)\rangle = |+\rangle|0\rangle$ , with the qubit in a  $\hat{\sigma}_x$  eigenstate  $|+\rangle$  and the oscillator in the vacuum state  $|0\rangle$ . The system is evolved freely, after which  $\hat{\sigma}_x$  is measured

$$\langle \hat{\sigma}_x \rangle = e^{-d(t)} \cos\phi(t), \quad (3)$$

where  $d(t) = (\alpha_+(t) - \alpha_-(t))^2/2 = 8\gamma^2 \sin^2(\omega t/2)/\omega^2$ , quantifying the overlap of the displaced oscillator states. Notably,  $d(t)$  only depends on the difference of displacements, it is therefore independent of the force  $\eta$  and the signal is only contained in the qubit phase  $\phi(t)$ . We calculate the quantum Fisher information (QFI) of the qubit with respect to the force  $\eta$

$$\mathcal{F}_\eta(t) = e^{-2d(t)} (\partial_\eta \phi(t))^2, \quad (4)$$

the inverse of which is the minimum uncertainty in estimating the force. The QFI reaches its maximum at integer multiples of the oscillator period,  $\tau = 2\pi/\omega$ , where the two oscillator trajectories reconverge at the origin (Fig. 1(b)) so that  $d(n\tau) = 0$ , meaning the qubit becomes fully decoupled from the oscillator. Thus the information is contained solely in the phase  $\phi(n\tau) = n\phi_0$ , where  $\phi_0 \equiv 8\pi\eta\gamma/\omega^2$ . Measuring  $\hat{\sigma}_x$  at such times optimally extracts this information, confirmed by

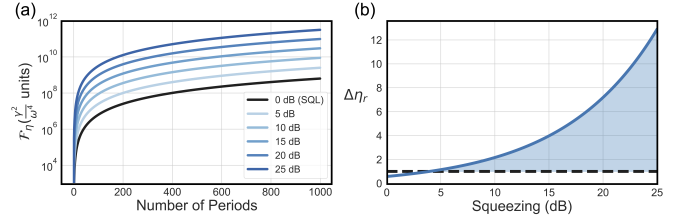


FIG. 2. (a) Quantum Fisher information of the qubit to sense the force  $\eta$  as a function of time. (b) The relative sensitivity of geometric protocol in comparison to standard free evolution scheme as a function of squeezing. Dashed line shows  $\Delta\eta_r = 1$  as a reference.

calculating the classical Fisher information  $\mathcal{F}_\eta^c(t) = (\partial_\eta \phi(t))^2 \sin^2 \phi(t) / (e^{2d(t)} - \cos^2 \phi(t))$ , which saturates the bound  $\mathcal{F}_\eta^c \leq \mathcal{F}_\eta$ :  $\mathcal{F}_\eta^c(n\tau) = \mathcal{F}_\eta(n\tau) = 64n^2\pi^2\gamma^2/\omega^4$ .

We emphasize that a *straightforward* application of squeezing to the oscillator state does not enhance sensitivity in this free-evolution scheme. Conjugating Eq. 2 with a squeezing operation  $\hat{S}(re^{2i\omega t})$  amplifies individual displacements  $\alpha_s(t) \rightarrow e^r \alpha_s(t)$  that contain information about the force  $\eta$ . However, optimal qubit measurement in Eqs. 3,4 is only sensitive to their difference  $d(t)$ , which is similarly amplified  $d(t) \rightarrow e^{2r} d(t)$  but carries no information about the force  $\eta$ , meanwhile the force-dependent phase  $\phi(t)$  remains unchanged.

*Geometric Protocol*— To exploit squeezing for enhanced sensitivity, we now present a sensing scheme that harnesses an additional geometrical phase, which converts the amplified path in oscillator phase space into a measurable qubit phase, enabling sensitivities beyond SQL. The protocol involves squeezing the oscillator degree of freedom and driving the qubit with  $\pi$ -pulses, both readily available in multiple platforms. The scheme is illustrated in Fig. 1(c),(d), with explicit calculations shown in supplemental material [55]. In step 1, we conjugate the free evolution with a squeezing operation to achieve amplification of the signal,

$$\hat{U}_{1,s} = e^{i\frac{\phi_0}{4}s} \hat{D}(2e^r \alpha_s). \quad (5)$$

In step 2, we apply two  $\pi$ -pulses to the qubit at times shown in Fig 1(c), implementing displacements

$$\hat{U}_{2,s} = \hat{D}(\alpha_s) \hat{D}(\beta_s) \hat{D}^\dagger(\alpha_s), \quad (6)$$

where  $\beta_s = 4i\gamma s/\omega$  is the displacement along the  $p$  axis. The evolution in the oscillator phase space is depicted in Fig. 1(d). To complete the loop, we repeat the first two steps, time shifted by  $\tau/2$ , obtaining

$$\begin{aligned} \hat{U}_{3,s} &= e^{i\frac{\phi_0}{4}s} \hat{D}^\dagger(2e^r \alpha_s), \\ \hat{U}_{4,s} &= \hat{U}_{2,s}^\dagger, \end{aligned} \quad (7)$$

Taken together, the total evolution traces a rectangular path in the phase space given by

$$\hat{U}_s = \hat{U}_{4,s} \hat{U}_{3,s} \hat{U}_{2,s} \hat{U}_{1,s} = e^{i\frac{\phi_0 T}{2}} \hat{I}, \quad (8)$$

where the total phase  $\phi_T = \phi_0 s + 4A_s$  and

$$A_s = 2\alpha_s(e^r - 1)\beta_s = 8(e^r - 1)s\gamma\eta/\omega^2 \quad (9)$$

is the geometrical contribution, equal to the area enclosed by the oscillator motion marked by the shaded region in Fig. 1(d). The oscillator state is shown at specific snapshots in time. The path will look different when viewed at different times; however, the area remains the same, highlighting its geometric nature. The placement of  $\pi$ -pulses is carefully chosen such that the enclosed area captures the enhanced signal  $\eta$  and is  $s$ -dependent to ensure that it is physical. The total evolution decouples the qubit and the oscillator, amounting to only a phase kickback on the qubit and identity operation on the oscillator, indicating that our protocol is independent of the initial oscillator state. This has the benefit of using higher temperature thermal states that are easy to prepare or logical states such as GKP that can aid in error corrected sensing. We therefore start in an arbitrary oscillator state with the qubit in  $|+\rangle$  superposition state, evolve under  $U_s$ , and perform an interference experiment similar to the free-evolution scheme by measuring  $\sigma_x$  of the qubit to extract the phase. Using Eq. 4, we calculate the QFI for the geometric protocol

$$\mathcal{F}_\eta^g = 64n^2(\pi + 4(e^r - 1))^2\gamma^2/\omega^4, \quad (10)$$

where  $n$  is the number of loops completed in the phase space. It is crucially dependent on the area enclosed in the phase space and therefore increases with the squeezing parameter  $r$ , thus confirming beyond-SQL scaling, as plotted in Fig 2(a). For  $r = 0$ , the geometric part vanishes, leaving the standard quantum limited measurement shown with the black line. To evaluate improvement in sensitivity with respect to the free-evolution protocol, we account for the longer duration of the geometric loop, which takes  $T_g = 3\tau$ , three times that of the free-evolution period. We compare the sensitivity of the geometric protocol  $\Delta\eta_g = 1/\sqrt{\mathcal{F}_\eta^g/(nT_g)}$ , with that of the free-evolution scheme  $\Delta\eta_0 = 1/\sqrt{\mathcal{F}_\eta(n\tau)/(n\tau)}$ . Figure 2(b) shows the relative sensitivity  $\Delta\eta_r = \Delta\eta_0/\Delta\eta_g$  as a function of squeezing, where  $\Delta\eta_r > 1$  indicates the gain obtained from using the geometric scheme. At low squeezing, the free-evolution scheme yields better sensitivity due to the shorter cycle time. However, beyond  $\approx 4$  dB of squeezing, the geometric contribution outperforms, highlighted by the shaded region. State-of-art platforms already achieve  $\sim 15$  dB of squeezing [56] corresponding to 4 fold improvement over SQL limited free evolution protocol.

Next, we apply our method to the case where squeezing is explicitly achieved via a sudden change in the oscillator frequency [57] from  $\omega$  to  $\omega'$ , which implements squeezing with strength  $r = \ln(\omega/\omega')/2$ , with protocol illustrated in Fig. 3(a). Evolving the oscillator at

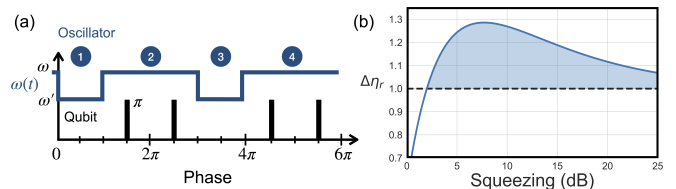


FIG. 3. (a) Sequence of operations for the geometric method with phase  $\theta = \int dt\omega(t)$ , where the squeezing is achieved by suddenly changing the oscillator frequency  $\omega(t)$  from  $\omega$  to  $\omega'$ . (b) Relative sensitivity of geometric protocol in comparison to standard free evolution with  $\omega'$  frequency as a function of squeezing.

a lower frequency  $\omega'$ , rescales both the displacement amplitude  $\alpha'_s = \alpha_s e^{4r}$ , and the phase collected per evolution  $\phi'_0 = \phi_0 e^{4r}$ . However, this exponential factor is trivial as it arises solely from evolving the oscillator at a lower frequency and not from squeezing. Steps 2 and 4 of our protocol remain unchanged, while steps 1 and 3 are rescaled as  $\hat{U}_{1,s} = e^{is\phi_0/4}\hat{D}(2\alpha_s e^{3r})$  and  $\hat{U}_{3,s} = e^{is\phi'_0/4}\hat{D}^\dagger(2\alpha_s e^{3r})$  [55]. The total relative phase is now  $\phi_T = \phi'_0 s + 4A_s$ , where the additional geometric contribution is  $A_s = 2\alpha_s(e^{3r} - 1)\eta\gamma/\omega^2$ . The factor  $e^{3r}$  arises purely from the oscillator trajectory in phase space and contributes to the total phase, enhancing the sensing performance. This is confirmed by the corresponding quantum Fisher information  $\mathcal{F}_\eta = 64n^2(e^{4r}\pi + 4(e^{3r} - 1))^2\gamma^2/\omega^4$ . The time taken for the total loop is now  $T_g = 2 \times 2\pi/\omega + 2\pi/\omega'$  as the oscillator spends one period with  $\omega'$  frequency and two periods in  $\omega$ . Although this is longer than the freely evolving the oscillator under lower frequency  $\omega'$ , the additional  $e^{3r}$  enhancement in phase improves the sensitivity. The relative sensitivity of the geometric protocol compared to free-evolution under  $\omega'$  is shown in Fig. 3(b), demonstrating up to  $\sim 30\%$  improvement for current experimentally achievable squeezing [57].

*Sensing in dispersively-coupled systems*— We now extend our method to dispersively coupled qubit-oscillator systems, which are widely realized in standard superconducting quantum devices using circuit quantum electrodynamics (cQED) architectures [1, 9, 58], where high-fidelity qubit readout is routinely available [59, 60]. In the dispersive regime, the effective Hamiltonian is given by

$$H_D/\hbar = \frac{\chi}{2}\hat{a}^\dagger\hat{a}\hat{\sigma}_z + i(\epsilon(t)\hat{a}^\dagger - \epsilon^*(t)\hat{a}), \quad (11)$$

where  $\chi$  is the dispersive shift and  $\epsilon(t)$  is the driving pulse on the resonator. The pulse amplitude  $\epsilon_0 = \max(\epsilon(t))$  is generally unknown a priori and was determined using a geometrical phase [45] which is SQL limited. We demonstrate that our protocol can be used to enhance this sensitivity beyond the SQL. Additionally, the same method can measure dispersive shift  $\chi$  surpassing SQL.

The procedure is illustrated in Fig. 4(b),(c), where we steer the system around a loop [55]. A related protocol for large spins, but without squeezing, was explored in Ref. [48]. In step 1, the cavity is strongly driven ( $\epsilon \gg \chi$ ) to generate a displacement  $\alpha = \int \epsilon(t)dt$ , along  $x$ , which is conjugated by free evolution  $\hat{R} = e^{-is\frac{\chi}{2}\hat{a}^\dagger\hat{a}}$

$$\hat{U}_1 = \hat{R}^\dagger \hat{D}(\alpha) \hat{R} = \hat{D}(\alpha e^{is\frac{\chi}{2}}), \quad (12)$$

where the time reversal of free evolution  $\hat{R}^\dagger$  is achieved by  $\pi$  pulses on the qubit. Subsequently, we conjugate the drive with squeezing to obtain amplification of the signal

$$\hat{U}_2 = \hat{S}^\dagger(r) \hat{D}(\alpha) \hat{S}(r) = \hat{D}(\alpha e^r). \quad (13)$$

Finally, we reverse the first and second unitary by applying the resonator drive with a phase shift of  $\pi$ , thereby closing the loop  $\hat{U} = \hat{U}_2^\dagger \hat{U}_1^\dagger \hat{U}_2 \hat{U}_1$ , as depicted in Fig. 4(b),(c). At the end of the process, the oscillator and qubit decouple, yielding  $\hat{U} = e^{is\phi/2} \hat{I}$ , with the relative phase on the qubit  $\phi = 4A$ , where  $A = \alpha^2 e^r \sin(\chi t/2)$  is the area enclosed in the parallelogram traversed by the oscillator in the phase space [55]. This phase is measured by a similar interference experiment by starting in an arbitrary oscillator state and qubit  $|\uparrow\rangle$  state. It is used to estimate the displacement to obtain the pulse amplitude or the dispersive coupling given that the other is known. The corresponding QFI using Eq. 4 after traversing  $n$  loops in the phase space

$$\begin{aligned} \mathcal{F}_\alpha &= (\partial_\alpha \phi)^2 = 64n^2 \alpha^2 e^{2r} \sin^2(\chi t/2), \\ \mathcal{F}_\chi &= (\partial_\chi \phi)^2 = 4n^2 t^2 \alpha^4 e^{2r} \cos^2(\chi t/2). \end{aligned} \quad (14)$$

Figure 4(d) shows the relative enhancement in sensitivity  $\Delta\alpha_r, \Delta\chi_r = e^r$ , as compared to SQL ( $r = 0$ ). Given experimentally demonstrated squeezing of 15 dB [56], the method obtains  $\sim 5$  times improvement over SQL for both pulse calibration and dispersive shift estimation.

**Robustness** — Preserving sensitivity under noise is crucial as realistic systems inevitably suffer from dissipation and decoherence. We show that the geometric nature of our protocol makes it resilient to qubit noise while retaining its independence of the oscillator's initial state. We numerically simulated the system under Markovian noise using a Lindblad master equation acting on both the oscillator and the qubit [61]. As a representative case, we analyze the inertial sensing protocol by interleaving the unitary steps  $\mathcal{U}_i(\bullet) = \hat{U}_i(\bullet)U_i^\dagger$ ,  $i \in \{1, \dots, 4\}$  with noise channel  $\mathcal{E}_t = e^{\mathcal{L}t}$ , where the Lindblad term is  $\partial_t \rho = \mathcal{L}\rho = \hat{L}\rho\hat{L}^\dagger - \frac{1}{2}(\hat{L}^\dagger\hat{L}\rho + \rho\hat{L}^\dagger\hat{L})$  and  $\rho$  is the joint system state. We consider a comprehensive list of six elementary noise processes: (i) boson loss  $\hat{L} = \sqrt{\lambda}\hat{a}$ , (ii) boson heating  $\hat{L} = \sqrt{\lambda}\hat{a}^\dagger$ , (iii) boson dephasing  $\hat{L} = \sqrt{\lambda}\hat{a}^\dagger\hat{a}$ , (iv) qubit decay  $\hat{L} = \sqrt{\lambda}\sigma^-$ , (v) qubit heating  $\hat{L} = \sqrt{\lambda}\sigma^+$ , and (vi) qubit dephasing  $\hat{L} = \sqrt{\lambda}\hat{\sigma}_z$ , where  $\lambda$  is the rate of noise. The noisy evolution is given by

$$\mathcal{E}_T = \mathcal{E}_\tau \circ \mathcal{U}_4 \circ \mathcal{E}_{\tau/2} \circ \mathcal{U}_3 \circ \mathcal{E}_\tau \circ \mathcal{U}_2 \circ \mathcal{E}_{\tau/2} \circ \mathcal{U}_1, \quad (15)$$

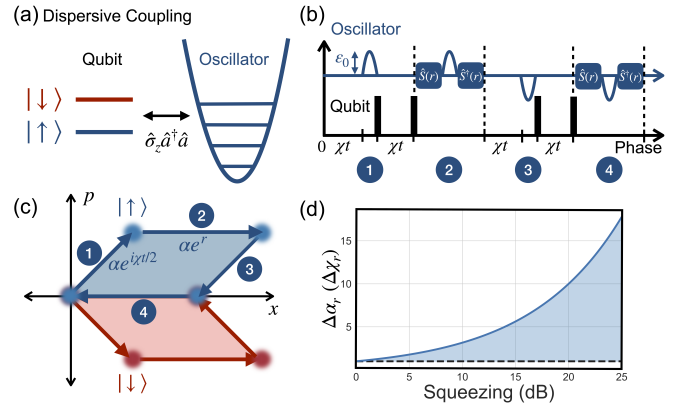


FIG. 4. (a) We consider dispersively coupled qubit-oscillator systems. (b) Sequence of operations on the oscillator and qubit for the geometric protocol and (c) the corresponding phase space evolution. (d) Relative sensitivity in comparison to SQL for estimating either the displacement  $\alpha$  or the dispersive coupling  $\chi$  as a function of squeezing.

where  $\circ$  represents the composition of quantum channels and each dissipative channel has the same duration as the corresponding unitary step.

For each noise channel, the Wigner function is shown at each step of the evolution in Fig. 5(a). The protocol demonstrates much stronger robustness to qubit noise than to bosonic noise. Bosonic noise perturbs the oscillator phase-space trajectory, distorting the area which corrupts the signal. The last column shows qubit state projected to the  $x - y$  Bloch plane, where the phase  $\phi$  encoding the signal (red arrow) is shown relative to the noiseless phase (blue arrow), highlighting the deviation under bosonic noise. By contrast, qubit decay (excitation) merely redistributes the population between  $|0\rangle$  and  $|1\rangle$ , leaving the oscillator's trajectory largely intact, while qubit dephasing commutes with the unitaries, producing an overall decay factor, we see that this leaves the angle and thus the signal largely intact, indicating robustness.

Finally, we examine the protocol's insensitivity to different initial oscillator states by considering five representative states: the vacuum state, coherent state  $\alpha = 1$ , thermal state  $n = 1$ , cat state  $n = 1$ , as well as the GKP logical state. Figure 5(b) shows the QFI for each noise channel. Consistent with the Wigner function analysis, the QFI for qubit channels is much higher than their bosonic counterpart. Importantly, the protocol retains its independence over the initial oscillator states near perfectly under qubit noise.

In summary, we introduced a quantum sensing protocol for qubit-oscillator systems that harnesses the geometrical phase to obtain sensitivities beyond the SQL. The method is resilient to qubit noise which can be a dominant source of error, offering practical advantages in real world applications. This work reveals another interesting aspect of the much-studied geometrical phases

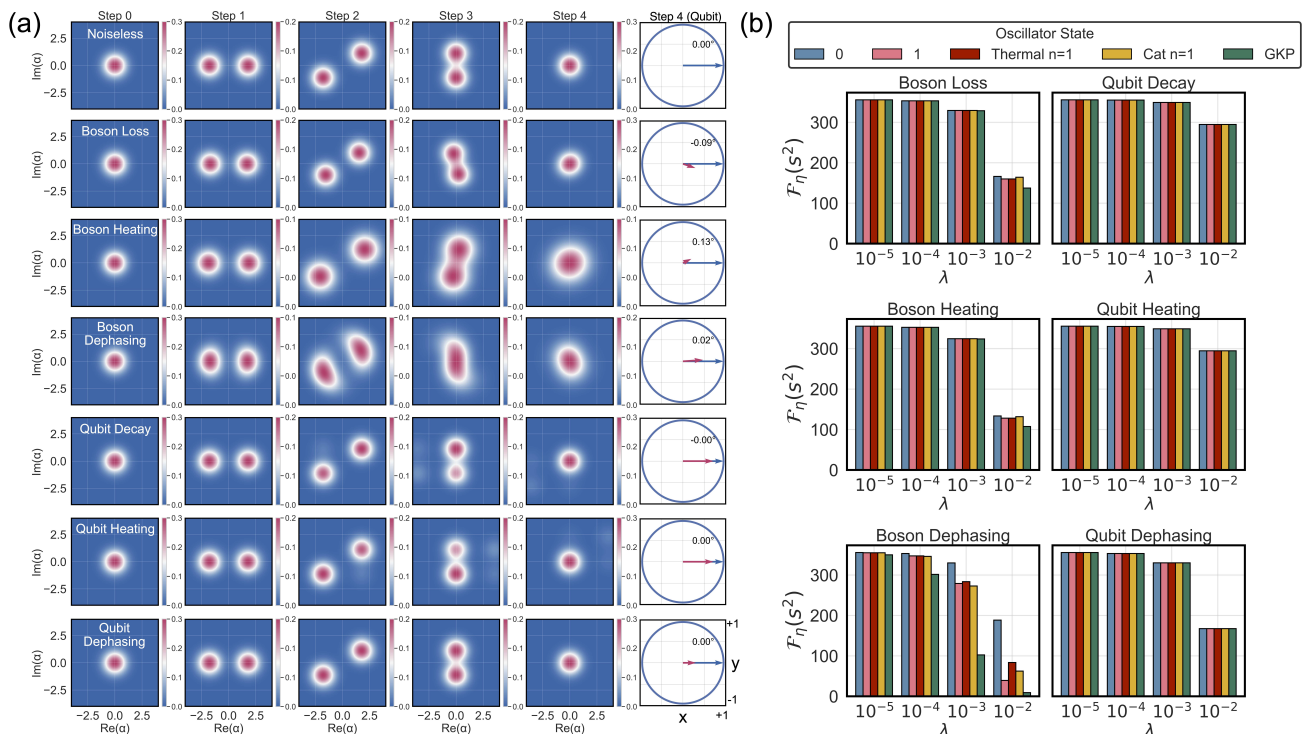


FIG. 5. Effect of noise for inertial force sensing. We consider typical parameters [16] where  $\omega = 1$ , qubit-oscillator coupling  $\gamma = 0.2$ , with 10 dB of squeezing, the force  $\eta = 10^{-5}$  and the fock space cutoff  $N = 200$ . (a) Wigner functions for the joint state at each step of the geometric protocol for all noise channels with strength  $\lambda = 0.05$ . The last column is the final qubit state projected to the  $x - y$  plane (marked by red arrow), with printed phase  $\phi$  relative to the noiseless case (shown with blue arrow). For visual clarity the vectors are drawn with  $100\times$ relative angle. (b) Numerical calculation of QFI for different initial states after 1 period of evolution for each noise channel as a function of increasing error rate  $\lambda$ .

and their natural intersection with beyond-SQL sensing, opening new possibilities in quantum metrology.

The authors thank Daniel Carney for fruitful discussions. This work is supported by a collaboration between the US DOE and other Agencies. WAdJ is supported by the U.S. Department of Energy, Office of Science, National Quantum Information Science Research Centers, Quantum Systems Accelerator. Additional support for NS is acknowledged from the “Embedding Quantum Computing into Manybody Frameworks for Strongly Correlated Molecular and Materials Systems” project, by the U.S. DOE, Office of Science, Office of Basic Energy Sciences, Division of Chemical Sciences, Geosciences, and Biosciences. T.R. and D.V. acknowledges funding supported by the U.S. Department of Energy, Office of Science, National Quantum Information Science Research Centers, Superconducting Quantum Materials and Systems Center (SQMS), under Contract No. 89243024CSC000002.

\* surinishchay@gmail.com

[1] A. Blais, R.-S. Huang, A. Wallraff, S. M. Girvin, and

- R. J. Schoelkopf, Cavity quantum electrodynamics for superconducting electrical circuits: An architecture for quantum computation, *Phys. Rev. A* **69**, 062320 (2004).  
 [2] D. Leibfried, B. DeMarco, V. Meyer, D. Lucas, M. Barrett, J. Britton, W. M. Itano, B. Jelenković, C. Langer, T. Rosenband, *et al.*, Experimental demonstration of a robust, high-fidelity geometric two ion-qubit phase gate, *Nature* **422**, 412 (2003).  
 [3] M. Aspelmeyer, T. J. Kippenberg, and F. Marquardt, Cavity optomechanics, *Rev. Mod. Phys.* **86**, 1391 (2014).  
 [4] S. Kolkowitz, A. C. Bleszynski Jayich, Q. P. Unterreithmeier, S. D. Bennett, P. Rabl, J. Harris, and M. D. Lukin, Coherent sensing of a mechanical resonator with a single-spin qubit, *Science* **335**, 1603 (2012).  
 [5] P. Lodahl, S. Mahmoodian, and S. Stobbe, Interfacing single photons and single quantum dots with photonic nanostructures, *Reviews of Modern Physics* **87**, 347–400 (2015).  
 [6] B. Rogers, N. Lo Gullo, G. De Chiara, G. M. Palma, and M. Paternostro, Hybrid optomechanics for quantum technologies, *Quantum Measurements and Quantum Metrology* **2**, 000010247820140002 (2014).  
 [7] Y. Chu and S. Gröblacher, A perspective on hybrid quantum opto- and electromechanical systems, *Applied Physics Letters* **117**, 150503 (2020).  
 [8] G. Kurizki, P. Bertet, Y. Kubo, K. Mølmer, D. Petrosyan, P. Rabl, and J. Schmiedmayer, Quantum technologies with hybrid systems, *Proceedings of the National*

- Academy of Sciences **112**, 3866 (2015).
- [9] A. Clerk, K. Lehnert, P. Bertet, J. Petta, and Y. Nakamura, Hybrid quantum systems with circuit quantum electrodynamics, *Nature Physics* **16**, 257 (2020).
- [10] D. Lee, K. W. Lee, J. V. Cady, P. Ovartchaiyapong, and A. C. B. Jayich, Topical review: spins and mechanics in diamond, *Journal of Optics* **19**, 033001 (2017).
- [11] J. Sinanan-Singh, G. L. Mintzer, I. L. Chuang, and Y. Liu, Single-shot quantum signal processing interferometry, *Quantum* **8**, 1427 (2024).
- [12] M. Scala, M. S. Kim, G. W. Morley, P. F. Barker, and S. Bose, Matter-wave interferometry of a levitated thermal nano-oscillator induced and probed by a spin, *Phys. Rev. Lett.* **111**, 180403 (2013).
- [13] C. Wan, M. Scala, G. W. Morley, A. A. Rahman, H. Ulbricht, J. Bateman, P. F. Barker, S. Bose, and M. S. Kim, Free nano-object ramsley interferometry for large quantum superpositions, *Phys. Rev. Lett.* **117**, 143003 (2016).
- [14] C. Wan, M. Scala, S. Bose, A. C. Frangeskou, A. A. Rahman, G. W. Morley, P. F. Barker, and M. S. Kim, Tolerance in the ramsley interference of a trapped nanodiamond, *Phys. Rev. A* **93**, 043852 (2016).
- [15] Z.-q. Yin, T. Li, X. Zhang, and L. M. Duan, Large quantum superpositions of a levitated nanodiamond through spin-optomechanical coupling, *Phys. Rev. A* **88**, 033614 (2013).
- [16] M. T. Johansson, G. K. Brennen, and J. Twamley, Macroscopic superpositions and gravimetry with quantum magnetomechanics, *Scientific reports* **6**, 37495 (2016).
- [17] O. Romero-Isart, L. Clemente, C. Navau, A. Sanchez, and J. I. Cirac, Quantum magnetomechanics with levitating superconducting microspheres, *Phys. Rev. Lett.* **109**, 147205 (2012).
- [18] V. Montenegro, Heisenberg-limited spin-mechanical gravimetry, *Physical Review Research* **7**, 013016 (2025).
- [19] J. Prat-Camps, C. Teo, C. C. Rusconi, W. Wieczorek, and O. Romero-Isart, Ultrasensitive inertial and force sensors with diamagnetically levitated magnets, *Phys. Rev. Appl.* **8**, 034002 (2017).
- [20] M. Canturk and A. Lupascu, Quadrature readout and generation of squeezed states of a harmonic oscillator using a qubit-based indirect measurement, *arXiv preprint arXiv:1704.04533* (2017).
- [21] T. M. Hoang, J. Ahn, J. Bang, and T. Li, Electron spin control of optically levitated nanodiamonds in vacuum, *Nature communications* **7**, 12250 (2016).
- [22] L. P. Neukirch, E. Von Haartman, J. M. Rosenholm, and A. Nick Vamivakas, Multi-dimensional single-spin nano-optomechanics with a levitated nanodiamond, *Nature Photonics* **9**, 653 (2015).
- [23] W. Ji, C. Xu, G. Qu, and D. Budker, Levitated sensor for magnetometry in ambient environment, *arXiv preprint arXiv:2504.21524* (2025).
- [24] S. Rani, X. Cao, A. E. Baptista, A. Hoffmann, and W. Pfaff, High-dynamic-range quantum sensing of magnons and their dynamics using a superconducting qubit, *Phys. Rev. Appl.* **23**, 064032 (2025).
- [25] J.-M. Pirkkalainen, S. Cho, F. Massel, J. Tuorila, T. Heikkilä, P. Hakonen, and M. Sillanpää, Cavity optomechanics mediated by a quantum two-level system, *Nature communications* **6**, 6981 (2015).
- [26] C. Eichler and J. R. Petta, Realizing a circuit analog of an optomechanical system with longitudinally coupled superconducting resonators, *Phys. Rev. Lett.* **120**, 227702 (2018).
- [27] T. Bera, S. Majumder, S. K. Sahu, and V. Singh, Large flux-mediated coupling in hybrid electromechanical system with a transmon qubit, *Communications Physics* **4**, 12 (2021).
- [28] C. A. Potts, R. C. Dekker, S. Deve, E. W. Strijbis, and G. A. Steele, Strong intrinsic longitudinal coupling in circuit quantum electrodynamics, *Phys. Rev. Lett.* **134**, 153603 (2025).
- [29] P.-M. Billangeon, J. S. Tsai, and Y. Nakamura, Circuit-qed-based scalable architectures for quantum information processing with superconducting qubits, *Phys. Rev. B* **91**, 094517 (2015).
- [30] J. R. Johansson, G. Johansson, and F. Nori, Optomechanical-like coupling between superconducting resonators, *Phys. Rev. A* **90**, 053833 (2014).
- [31] S. Chen, H. Fukuda, T. Inada, T. Moroi, T. Nitta, and T. Sichanugrist, Search for qcd axion dark matter with transmon qubits and quantum circuit, *Phys. Rev. D* **110**, 115021 (2024).
- [32] C. Braggio, L. Balembois, R. Di Vora, Z. Wang, J. Travesedo, L. Pallegoix, G. Carugno, A. Ortolan, G. Ruoso, U. Gambardella, D. D'Agostino, P. Bertet, and E. Flurin, Quantum-enhanced sensing of axion dark matter with a transmon-based single microwave photon counter, *Phys. Rev. X* **15**, 021031 (2025).
- [33] A. V. Dixit, S. Chakram, K. He, A. Agrawal, R. K. Naik, D. I. Schuster, and A. Chou, Searching for dark matter with a superconducting qubit, *Phys. Rev. Lett.* **126**, 141302 (2021).
- [34] A. Agrawal, A. V. Dixit, T. Roy, S. Chakram, K. He, R. K. Naik, D. I. Schuster, and A. Chou, Stimulated emission of signal photons from dark matter waves, *Phys. Rev. Lett.* **132**, 140801 (2024).
- [35] F. Zhao, Z. Li, A. V. Dixit, T. Roy, A. Vrajitoarea, R. Banerjee, A. Anferov, K.-H. Lee, D. I. Schuster, and A. Chou, Flux-tunable cavity for dark matter detection, *Phys. Rev. Lett.* **135**, 201002 (2025).
- [36] C. L. Degen, F. Reinhard, and P. Cappellaro, Quantum sensing, *Rev. Mod. Phys.* **89**, 035002 (2017).
- [37] G. Tóth and I. Apellaniz, Quantum metrology from a quantum information science perspective, *Journal of Physics A: Mathematical and Theoretical* **47**, 424006 (2014).
- [38] D. Carney, P. C. E. Stamp, and J. M. Taylor, Tabletop experiments for quantum gravity: a user's manual, *Classical and Quantum Gravity* **36**, 034001 (2019).
- [39] S. Bose, I. Fuentes, A. A. Geraci, S. M. Khan, S. Qvarfort, M. Rademacher, M. Rashid, M. Toroš, H. Ulbricht, and C. C. Wanjura, Massive quantum systems as interfaces of quantum mechanics and gravity, *Rev. Mod. Phys.* **97**, 015003 (2025).
- [40] M. Rademacher, J. Millen, and Y. L. Li, Quantum sensing with nanoparticles for gravimetry: when bigger is better, *Advanced Optical Technologies* **9**, 227 (2020).
- [41] S. C. Burd, R. Srinivas, J. J. Bollinger, A. C. Wilson, D. J. Wineland, D. Leibfried, D. H. Slichter, and D. T. C. Allcock, Quantum amplification of mechanical oscillator motion, *Science* **364**, 1163 (2019), <https://www.science.org/doi/pdf/10.1126/science.aaw2884>.
- [42] S. Chaturvedi, M. S. Sriram, and V. Srinivasan, Berry's phase for coherent states, *Journal of Physics A: Mathematical and General* **20**, L1071 (1987).

- [43] M. Pechal, S. Berger, A. A. Abdumalikov, J. M. Fink, J. A. Mlynek, L. Steffen, A. Wallraff, and S. Filipp, Geometric phase and nonadiabatic effects in an electronic harmonic oscillator, *Phys. Rev. Lett.* **108**, 170401 (2012).
- [44] G. Vacanti, R. Fazio, M. S. Kim, G. M. Palma, M. Paternostro, and V. Vedral, Geometric-phase backaction in a mesoscopic qubit-oscillator system, *Phys. Rev. A* **85**, 022129 (2012).
- [45] A. Eickbusch, V. Sivak, A. Z. Ding, S. S. Elder, S. R. Jha, J. Venkatraman, B. Royer, S. M. Girvin, R. J. Schoelkopf, and M. H. Devoret, [Fast universal control of an oscillator with weak dispersive coupling to a qubit](#) (2022).
- [46] X. Wang and P. Zanardi, Simulation of many-body interactions by conditional geometric phases, *Phys. Rev. A* **65**, 032327 (2002).
- [47] C. Song, S.-B. Zheng, P. Zhang, K. Xu, L. Zhang, Q. Guo, W. Liu, D. Xu, H. Deng, K. Huang, *et al.*, Continuous-variable geometric phase and its manipulation for quantum computation in a superconducting circuit, *Nature communications* **8**, 1061 (2017).
- [48] M. T. Johnsson, N. R. Mukty, D. Burgarth, T. Volz, and G. K. Brennen, Geometric pathway to scalable quantum sensing, *Phys. Rev. Lett.* **125**, 190403 (2020).
- [49] D. Gottesman, A. Kitaev, and J. Preskill, Encoding a qubit in an oscillator, *Phys. Rev. A* **64**, 012310 (2001).
- [50] A. L. Grimsmo and S. Puri, Quantum error correction with the gottesman-kitaev-preskill code, *PRX Quantum* **2**, 020101 (2021).
- [51] Y. Liu, S. Singh, K. C. Smith, E. Crane, J. M. Martyn, A. Eickbusch, A. Schuckert, R. D. Li, J. Sinanan-Singh, M. B. Soley, T. Tsunoda, I. L. Chuang, N. Wiebe, and S. M. Girvin, Hybrid oscillator-qubit quantum processors: Instruction set architectures, abstract machine models, and applications, *PRX Quantum* [10.1103/PRXQuantum.X.YYYYYY](#) (2025).
- [52] D. Leibfried, R. Blatt, C. Monroe, and D. Wineland, Quantum dynamics of single trapped ions, *Rev. Mod. Phys.* **75**, 281 (2003).
- [53] P. C. Haljan, K.-A. Brickman, L. Deslauriers, P. J. Lee, and C. Monroe, Spin-dependent forces on trapped ions for phase-stable quantum gates and entangled states of spin and motion, *Phys. Rev. Lett.* **94**, 153602 (2005).
- [54] A. Sørensen and K. Mølmer, Entanglement and quantum computation with ions in thermal motion, *Phys. Rev. A* **62**, 022311 (2000).
- [55] Supplemental material, See Supplemental material at [URL or journal link] for details (2025).
- [56] Y. Cai, X. Deng, L. Zhang, Z. Ni, J. Mai, P. Huang, P. Zheng, L. Hu, S. Liu, Y. Xu, and D. Yu, [Quantum squeezing amplification with a weak kerr nonlinear oscillator](#) (2025), [arXiv:2503.08197 \[quant-ph\]](#).
- [57] M. Xin, W. S. Leong, Z. Chen, Y. Wang, and S.-Y. Lan, Rapid quantum squeezing by jumping the harmonic oscillator frequency, *Phys. Rev. Lett.* **127**, 183602 (2021).
- [58] P. Krantz, M. Kjaergaard, F. Yan, T. P. Orlando, S. Gustavsson, and W. D. Oliver, A quantum engineer's guide to superconducting qubits, *Applied Physics Reviews* **6**, 021318 (2019).
- [59] Y. Sunada, S. Kono, J. Ilves, S. Tamate, T. Sugiyama, Y. Tabuchi, and Y. Nakamura, Fast readout and reset of a superconducting qubit coupled to a resonator with an intrinsic purcell filter, *Phys. Rev. Appl.* **17**, 044016 (2022).
- [60] T. Kim, T. Roy, X. You, A. C. Li, H. Lamm, O. Pronitchev, M. Bal, S. Garattoni, F. Crisa, D. Bafia, *et al.*, Ultracoherent superconducting cavity-based multi-qubit platform with error-resilient control, [arXiv preprint arXiv:2506.03286](#) (2025), [2506.03286](#).
- [61] J. Hastrup, K. Park, R. Filip, and U. L. Andersen, Unconditional preparation of squeezed vacuum from rabi interactions, *Phys. Rev. Lett.* **126**, 153602 (2021).

# Supplemental Material on “Quantum Sensing using Geometric Phase in Qubit-Oscillator Systems”

Nishchay Suri,<sup>1,\*</sup> Zhihui Wang,<sup>2,3</sup> Tanay Roy,<sup>4</sup> Davide Venturelli,<sup>2,3</sup> and Wibe Albert de Jong<sup>1</sup>

<sup>1</sup>*Applied Mathematics and Computational Research Division,*

*Lawrence Berkeley National Laboratory, Berkeley, California 94720, USA*

<sup>2</sup>*Quantum Artificial Intelligence Laboratory, NASA Ames Research Center, Moffett Field, CA 94035, USA*

<sup>3</sup>*USRA Research Institute for Advanced Computer Science, Mountain View, California 94043, USA*

<sup>4</sup>*Superconducting Quantum Materials and Systems (SQMS) Center,  
Fermi National Accelerator Laboratory (FNAL), Batavia, IL 60510, USA*

## LONGITUDINALLY COUPLED QUBIT-OSCILLATOR SYSTEMS

### Free Evolution

The Hamiltonian of the coupled qubit oscillator system in the lab frame is given by

$$\frac{H_L}{\hbar} = -\frac{\omega_q}{2}\hat{\sigma}_z + \omega\hat{a}^\dagger\hat{a} + \gamma(\hat{a} + \hat{a}^\dagger)\hat{\sigma}_z + \eta(\hat{a} + \hat{a}^\dagger), \quad (\text{S1})$$

where  $\eta = F\frac{1}{\sqrt{2m\omega\hbar}}$  and  $F$  is a general force ( $F = mg$  for gravity). We do our entire analysis in the rotating frame  $U_0(t) = e^{-i(\frac{\omega_q}{2}\hat{\sigma}_z - \omega\hat{a}^\dagger\hat{a})t}$  where the Hamiltonian now is given by

$$H(t) = (\hat{a}e^{-i\omega t} + \hat{a}^\dagger e^{i\omega t})(\eta + \gamma\hat{\sigma}_z), \quad (\text{S2})$$

where  $H$  is in units of  $\hbar$ . Notice that this is a time dependent periodic Hamiltonian, however we can write its exact solution using Floquet framework. The harmonics of the system are given by  $H_0 = 0$ ,  $H_{+1} = \hat{a}^\dagger(\eta + \gamma\hat{\sigma}_z)$  and  $H_{-1} = \hat{a}(\eta + \gamma\hat{\sigma}_z)$ . Using Floquet theory, the total evolution of the system is given by

$$U(t, t_0) = e^{-iK(t)}e^{-iH_F(t-t_0)}e^{+iK(t_0)}, \quad (\text{S3})$$

where the Floquet Hamiltonian is

$$H_F = -\frac{1}{\omega}(\eta + \gamma\hat{\sigma}_z)^2 \quad (\text{S4})$$

and the micromotion operator

$$K(t) = \frac{1}{i\omega}(\hat{a}^\dagger e^{i\omega t} - \hat{a}e^{-i\omega t})(\eta + \gamma\hat{\sigma}_z). \quad (\text{S5})$$

The Floquet Hamiltonian only operates on the qubit, and as a result it commutes with micromotion operator  $[H_F, K(t)] = 0$ . Moreover, everything commutes with  $\hat{\sigma}_z$ , we can work in its eigenbasis  $|s\rangle \in \{|\uparrow\rangle, |\downarrow\rangle\}$ , corresponding to eigenvalues  $s = \pm 1$ . Defining  $\alpha_s = (\eta + \gamma s)/\omega$ , the total evolution becomes

$$U_s(t, t_0) = e^{i\frac{2\eta\gamma s}{\omega}(t-t_0)}\hat{D}^\dagger(\alpha_s e^{i\omega t})\hat{D}(\alpha_s e^{i\omega t_0}). \quad (\text{S6})$$

Starting at  $t_0 = 0$  the evolution is

$$U_s(t, 0) = e^{is\phi(t)/2}\hat{D}(\alpha_s(t)), \quad (\text{S7})$$

where  $\phi(t) = 4\eta\gamma(\omega t - \sin\omega t)/\omega$  and  $\alpha_s(t) = \alpha_s(1 - e^{i\omega t})$ .

*Free evolution protocol*— We start with the initial state

$$|\psi(0)\rangle = \frac{1}{\sqrt{2}}(|\uparrow\rangle + |\downarrow\rangle) \otimes |0\rangle, \quad (\text{S8})$$

and evolve the system under the free evolution Hamiltonian given above and obtain

$$|\psi(t)\rangle = \frac{1}{\sqrt{2}}(|+\rangle U_+(t)|0\rangle + |-\rangle U_-(t)|0\rangle), \quad (\text{S9})$$

where the reduced state of the qubit is

$$\rho_q(t) = \frac{1}{2} \begin{bmatrix} 1 & e^{-i\phi(t)} \langle \alpha_-(t) | \alpha_+(t) \rangle \\ e^{i\phi(t)} \langle \alpha_+(t) | \alpha_-(t) \rangle & 1 \end{bmatrix}. \quad (\text{S10})$$

Measuring  $\hat{\sigma}_x$  of the qubit state in fact directly measures this overlap as

$$\langle \hat{\sigma}_x \rangle = \frac{1}{2} (e^{-i\phi(t)} \langle \alpha_-(t) | \alpha_+(t) \rangle + e^{i\phi(t)} \langle \alpha_+(t) | \alpha_-(t) \rangle) = \cos(\phi(t)) e^{-d(t)}, \quad (\text{S11})$$

where  $d(t) = 2(\alpha_- - \alpha_+)^2 \sin^2(\omega t/2)$  is the geometric part.

*Fisher Information*— We now calculate the quantum Fisher information for the qubit with respect to  $\eta$  and obtain

$$\mathcal{F}_\eta(t) = (\partial_\eta \phi(t))^2 e^{-2d(t)}. \quad (\text{S12})$$

To check if our measurement of  $\hat{\sigma}_x$  is optimal we calculate the classical Fisher information given by

$$\mathcal{F}_\eta^c(t) = \frac{\sin^2(\phi(t))}{e^{2d(t)} - \cos^2(\phi(t))} (\partial_\eta \phi(t))^2. \quad (\text{S13})$$

Since  $d(t)$  is a positive function, the QFI is maximized when  $d(t) = 0$ . Moreover, the classical Fisher information saturates the bound when  $d(t) = 0$  which is when it extracts the maximum information contained in the system. This happens at integer time period of the oscillator when the qubit and oscillator are decoupled and the damping factor vanishes at  $\omega t_n = 2n\pi$ . Putting in all the values we get for a general time

$$\mathcal{F}_\eta(t) = 16 \frac{\gamma^2}{\omega^4} (\omega t - \sin \omega t)^2 e^{-16 \frac{\gamma^2}{\omega^2} \sin^2(\omega t/2)}. \quad (\text{S14})$$

and at integer times

$$\mathcal{F}_\eta(t_n) = 64n^2 \frac{\gamma^2 \pi^2}{\omega^4}. \quad (\text{S15})$$

*Squeezing*— Let us investigate what happens when we squeeze and anti-squeeze to amplify displacement, this is done with the transformation  $\hat{S}^\dagger(re^{2i\omega t})U(t,0)\hat{S}(re^{2i\omega t}) = e^{is\phi(t)/2}\hat{D}(e^r\alpha_s(t))$ . The phase of the qubit is unaltered, but the displacement is amplified. However, since the qubit only measures overlap of the displacements, this only leads to the amplifying the force independent overall factor in Fisher information, where  $d(t) \rightarrow e^r d(t)$ , which is maximized when  $d(t) = 0$  and therefore, does not aid in sensing.

### Geometric Protocol

We now describe our geometric sensing protocol that encodes the signal in geometric phase that depends on the area traversed by the oscillator in its phase space. We follow the scheme presented in the main text in Fig. 2(a), with the protocol divided into four parts. We analyze each part of the cycle separately.

1. Time:  $0 - \tau/2$ . We have the total evolution as the free evolution of the oscillator conjugated by the squeezing operation given by  $U_{1,s}(t, t_0) = \hat{S}^\dagger(re^{i2\omega t})U_s(t, t_0)\hat{S}(re^{i2\omega t_0})$ , where the squeezing phase comes from being in the rotating frame. We obtain

$$U_{1,s} = \hat{S}^\dagger(r)U_s(\tau/2, 0)\hat{S}(r) = e^{i\frac{\phi_0}{4}s}\hat{D}(2e^r\alpha_s) \quad (\text{S16})$$

where  $\phi_0 = 8\pi\gamma\eta/\omega^2$ .

2. Time:  $\tau/2 - 3\tau/2$ . We now have free evolution with  $\pi$  pulses on the qubit, effectively reversing the sign of the spin. The total unitary for the second step is therefore given by

$$\begin{aligned} U_{2,s} &= U_s(3\tau/2, 5\tau/4)U_{-s}(5\tau/4, 3\tau/4)U_s(3\tau/4, 3\tau/2) \\ &= \left( e^{is\phi_0/4}\hat{D}(i\alpha_s)\hat{D}(-\alpha_s) \right) \left( e^{-is\phi_0/2}\hat{D}(-i\alpha_{-s})\hat{D}(-i\alpha_{-s}) \right) \left( e^{is\phi_0/4}\hat{D}(\alpha_s)\hat{D}(i\alpha_s) \right) \\ &= \hat{D}(\alpha_s)\hat{D}(\beta_s)\hat{D}^\dagger(\alpha_s), \end{aligned} \quad (\text{S17})$$

where  $\beta_s = 2i(\alpha_s - \alpha_{-s}) = 4i\gamma s/\omega$ .

3. Time:  $3\tau/2 - 2\tau$ . Similar to step 1, we again conjugate the free evolution with squeezing and anti-squeezing, therefore, the unitary for general time is given by  $U_{3,s}(t, t_0) = \hat{S}^\dagger(re^{i2\omega t})U_s(t, t_0)\hat{S}(re^{i2\omega t_0})$ , obtaining

$$U_{3,s} = \hat{S}^\dagger(r)U_s(2\tau, 3\tau/2)\hat{S}(r) = e^{i\frac{\phi_0}{4}s}\hat{D}^\dagger(2e^r\alpha_s). \quad (\text{S18})$$

4. Time:  $2\tau - 3\tau$ . Similar to step 2, we again have  $\pi$  pulses reversing the sign of spin. The total unitary for step 4 is given as

$$\begin{aligned} U_{4,s} &= U_s(3\tau, 11\tau/4) U_{-s}(9\tau/4, 11\tau/4) U_s(9\tau/4, 2\tau) \\ &= \left( e^{is\phi_0/4}\hat{D}(-i\alpha_s)\hat{D}(\alpha_s) \right) \left( e^{-is\phi_0/2}\hat{D}(i\alpha_{-s})\hat{D}(i\alpha_{-s}) \right) \left( e^{is\phi_0/4}\hat{D}(-\alpha_s)\hat{D}(-i\alpha_s) \right) \\ &= \hat{D}^\dagger(\alpha_s)\hat{D}^\dagger(\beta_s)\hat{D}(\alpha_s), \end{aligned} \quad (\text{S19})$$

The total evolution is given by the unitary

$$\begin{aligned} U_{T,s} &= U_{4,s}U_{3,s}U_{2,s}U_{1,s} \\ &= e^{is\phi_0} \left( \hat{D}^\dagger(\alpha_s)\hat{D}^\dagger(\beta_s)\hat{D}(\alpha_s) \right) \hat{D}^\dagger(2e^r\alpha_s) \left( \hat{D}(\alpha_s)\hat{D}(\beta_s)\hat{D}^\dagger(\alpha_s) \right) \hat{D}(2e^r\alpha_s) \\ &= e^{i\frac{\phi_g}{2}} \hat{I} \end{aligned} \quad (\text{S20})$$

where the phase of our geometric protocol is  $\phi_T = \phi_0s + 4A_s$ , where the area  $A_s = 2\alpha_s(e^r - 1)\beta_s = 8(e^r - 1)s\gamma\eta/\omega^2$  is geometrical phase equal to the area of the loop traversed in the oscillator phase space. Mathematically, the last equation can be simplified by using commutation of displacements  $\hat{D}(\alpha)\hat{D}(\beta) = e^{i\text{Im}(\alpha\beta^*)}\hat{D}(\alpha + \beta)$ . Thus, the phase collected after  $n$  loops is  $n\phi_g = 8n(\pi + 4(e^r - 1))\gamma\eta/\omega^2$ . Using Eq. S12 to calculate the QFI, we obtain

$$\mathcal{F}_\eta = 64n^2 \frac{\gamma^2}{\omega^4} (\pi + 4(e^r - 1))^2, \quad (\text{S21})$$

where each loop takes  $3\tau$  time period.

### Squeezing with frequency change

One of experimentally feasible ways of obtaining squeezing is to suddenly change the oscillator frequency from  $\omega$  to  $\omega'$ . The Hamiltonian changes from  $H = \omega\hat{a}^\dagger\hat{a}$  to  $H' = \omega'\hat{a}'^\dagger\hat{a}'$ , where the annihilation and creation operators undergo a Bogoliubov transformation  $a' = \hat{S}^\dagger(r)a\hat{S}(r)$ , where the squeezing strength is  $r = \ln(\omega/\omega')/2$ . We now analyze our geometric protocol when the squeezing operation is applied using this sudden frequency change as shown in main text in Fig 3(a). The Hamiltonian in the Lab frame is now given as  $H_L/\hbar = -\frac{\omega_s}{2}\hat{\sigma}_z + \omega_t\hat{a}_t^\dagger\hat{a}_t + (\hat{a}_t^\dagger + \hat{a}_t)(\eta + \gamma s)$ , where  $\hat{a}_t = \hat{a}, \hat{a}'$  and  $\omega_t = \omega, \omega'$  for appropriate times  $t$  consistent with Fig. 3(a). Since, the Hamiltonian and operators change piecewise, we move to the rotating frame  $U_0 = e^{-i\frac{\omega_s t}{2}\hat{\sigma}_z} e^{i\theta_t\hat{a}_t^\dagger\hat{a}_t}$ , where  $\theta_t = \int_0^t dt'\omega_{t'}$  is the total oscillator phase collected at time  $t$ . Using the transformation,  $H = U_0H_LU_0^\dagger - iU_0\dot{U}_0^\dagger$ , the Hamiltonian in rotating frame is

$$H_t = (\hat{a}_t e^{-i\theta_t} + \hat{a}_t^\dagger e^{i\theta_t})(\eta + \gamma s). \quad (\text{S22})$$

When the frequency is only changed in a piecewise manner, the qualitative dynamics is the same as before, with the phase and displacement change appropriately with the frequency. For instance, free evolution of the oscillator with  $\omega'$  frequency is given by  $U'_s(t, 0) = e^{is\phi'(t)/2}\hat{D}(\alpha'_s(t))$ , where  $\phi'(t) = 4\eta\gamma(\omega't - \sin\omega't)/\omega'$  and  $\alpha'_s(t) = \alpha'_s(1 - e^{i\omega't})$  and  $\alpha'_s = (\eta + \gamma s)/\omega'$ . Since  $\omega' = \omega e^{-2r}$ , the phase collected at the end of one cycle is four times that with frequency  $\omega$ :  $\phi'_0 = \phi_0 e^{4r}$  and the displacement is amplified  $\alpha'_s = \alpha_s e^{2r}$ . The second and fourth steps remain unaltered, while the first and third steps become

1. Time:  $0 - \tau/2$ . We have the free evolution of the oscillator with frequency  $\omega'$ , conjugated by squeezing operation coming from the sudden change  $U_{1,s} = \hat{S}^\dagger(re^{i2\omega t})U'_s\hat{S}(re^{i2\omega t_0})$ , obtaining

$$U_{1,s} = e^{i\frac{\phi_0}{4}e^{4r}s}\hat{D}(2\alpha_s e^{3r}). \quad (\text{S23})$$

2. Time:  $3\tau/2 - 2\tau$ . Similarly we obtain

$$U_{3,s} = e^{i\frac{\phi_0}{4}e^{4r}s} \hat{D}^\dagger(2\alpha_s e^{3r}). \quad (\text{S24})$$

The total evolution is similarly given by

$$U_{T,s} = e^{i\frac{\phi_T}{2}s} \hat{I}, \quad (\text{S25})$$

where the total phase is  $\phi_T = e^{4r}\phi_0 + 4A_s$ , where the area is  $A = 2\alpha_s(e^{3r} - 1)\beta_s = 8(e^{3r} - 1)\eta\gamma/\omega^2$ . Substituting this into the QFI expression,

$$\mathcal{F}_\eta = 64n^2 \frac{\gamma^2}{\omega^4} (e^{4r}\pi + 4(e^{3r} - 1))^2, \quad (\text{S26})$$

and the time period per evolution is given by  $T_g = \frac{2\pi}{\omega} \times 2 + \frac{2\pi}{\omega'} = \frac{2\pi}{\omega} (2 + e^{2r})$ .

## DISPERSIVELY COUPLED QUBIT-OSCILLATOR SYSTEMS

In typical cavity QED systems, the qubit is transversally coupled to the cavity. In the dispersive limit, the qubit-resonator coupling is much smaller than their frequency difference, with the effective Hamiltonian given by

$$H = \frac{\chi}{2} \hat{\sigma}_z \hat{a}^\dagger \hat{a} + i\epsilon(t) \hat{a}^\dagger - i\epsilon^*(t) \hat{a}, \quad (\text{S27})$$

where  $\chi$  is the dispersive shift and  $\epsilon(t)$  is the drive on the resonator. When there is no drive/pulse on the resonator, the free evolution is given by  $\hat{R}_\theta = e^{-is\frac{\theta}{2}\hat{a}^\dagger\hat{a}}$ , where  $\theta = \chi t$ . We can drive the resonator by applying a pulse  $\epsilon(t)$ , displacing it by  $\hat{D}(\alpha)$ , where  $\alpha = \int dt' \epsilon(t')$ . We now consider the following operations

1. First, we implement a drive conjugated by free evolution

$$U_1 = \hat{R}_\theta^\dagger \hat{D}(\alpha) \hat{R}_\theta = \hat{D}(\alpha e^{is\frac{\theta}{2}}), \quad (\text{S28})$$

where  $\hat{R}_\theta^\dagger$  is implemented by conjugating the free evolution  $\hat{R}_\theta$  two  $\pi$  pulses, reversing the sign of qubit.

2. Next, we have drive implementing the real displacement, conjugated by squeezing

$$U_2 = \hat{S}^\dagger(r) \hat{D}(\alpha) \hat{S}(r) = \hat{D}(\alpha e^r). \quad (\text{S29})$$

3. We reverse the first unitary by applying drive with  $\pi$  phase

$$U_3 = \hat{R}_\theta^\dagger \hat{D}(-\alpha) \hat{R}_\theta = \hat{D}^\dagger(\alpha e^{is\frac{\theta}{2}}). \quad (\text{S30})$$

4. Similarly, we reverse the second step, completing the loop

$$U_4 = \hat{S}^\dagger(r) \hat{D}(-\alpha) \hat{S}(r) = \hat{D}^\dagger(\alpha e^r). \quad (\text{S31})$$

Finally, we obtain the total evolution

$$U = U_4 U_3 U_2 U_1 = e^{i\phi_s/2}, \quad (\text{S32})$$

where the geometric phase  $\phi_s = 4\alpha^2 e^r \sin(s\chi t/2)$ . Since  $s = \pm 1$ , we can just simplify the expression to the form we have been using in the paper

$$U = e^{i s \phi/2}, \quad (\text{S33})$$

where  $\phi = 4\alpha^2 e^r \sin(\chi t/2)$ . We can now use our standard formula to obtain the QFI for both the displacement which can be used to obtain the pulse amplitude and the dispersive coupling after  $n$  loops

$$\mathcal{F}_\alpha = (\partial_\alpha \phi)^2 = 64n^2 \alpha^2 e^{2r} \sin^2(\chi t/2), \quad (\text{S34})$$

$$\mathcal{F}_\chi = (\partial_\chi \phi)^2 = 4n^2 t^2 \alpha^4 e^{2r} \cos^2(\chi t/2). \quad (\text{S35})$$

---

\* surinishchay@gmail.com